Analysis of Transonic Limit Cycle Oscillations under Uncertainty

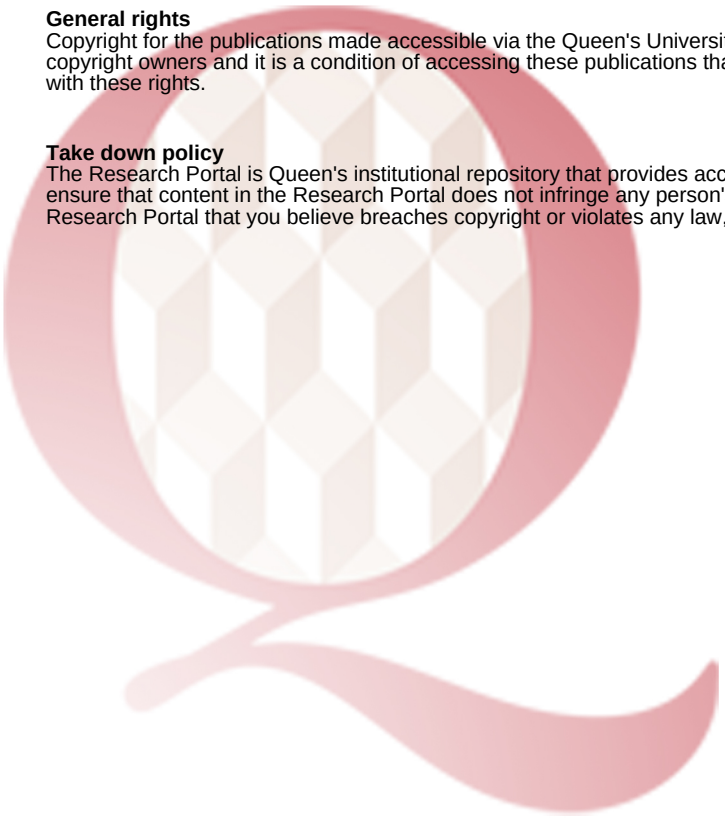

Analysis of Transonic Limit Cycle Oscillations under Uncertainty

R. Hayes* and S. Marques† and W. Yao‡

Queen's University Belfast, Belfast, BT9 5AH, Northern Ireland

For the computation of limit cycle oscillations (LCO) at transonic speeds, CFD is required to capture the nonlinear flow features present. The Harmonic Balance method provides an effective means for the computation of LCOs and this paper exploits its efficiency to investigate the impact of variability (both structural and aerodynamic) on the aeroelastic behaviour of a 2 *dof* aerofoil. A Harmonic Balance inviscid CFD solver is coupled with the structural equations and is validated against time marching analyses. Polynomial chaos expansions are employed for the stochastic investigation as a faster alternative to Monte Carlo analysis. Adaptive sampling is employed when discontinuities are present. Uncertainties in aerodynamic parameters are looked at first followed by the inclusion of structural variability. Results show the nonlinear effect of Mach number and it's interaction with the structural parameters on supercritical LCOs. The bifurcation boundaries are well captured by the polynomial chaos.

Nomenclature

Latin symbols

$\mathbf{D}$	Harmonic Balance operator
M	Mach number
$\mathbf{L}_n$	L2 norm of residual
N_H	number of harmonics in Fourier expansion
$\mathbf{R}$	CFD flux residual
t	time
U	velocity
V_s	velocity index
$\mathbf{W}$	vector of conserved flow variables
$\mathbf{Y}$	pitch/plunge displacements and velocities

Greek Symbols

ρ	air density
τ	pseudo time
ω	fundamental solution frequency

Subscripts and Superscripts

$()_\alpha$	in pitch *dof*
$()_h$	in plunge *dof*
$()_\mathbf{s}$	state-space matrix
$()_0$	reference value
$()_\infty$	free-stream value

*PhD student, School of Mechanical & Aerospace Engineering, QUB, Belfast, Student member AIAA. rhayes04@qub.ac.uk

†Lecturer, School of Mechanical & Aerospace Engineering, QUB, Belfast, Senior member AIAA. s.marques@qub.ac.uk

‡Research Fellow, School of Mechanical & Aerospace Engineering, QUB, Belfast, Senior member AIAA. w.yao@qub.ac.uk

I. Introduction

Flutter testing is a crucial stage in the design of an aircraft; however, flight testing can be both costly and dangerous. Hence simulation is becoming more influential in the design and certification of modern aircraft. Due to the range of flow conditions experienced within the flight envelope and the intrinsic variability associated with the manufacture of an aircraft, the need for stochastic analysis in the computational model is clear.[1]

Marques *et al* demonstrated that structural variability can have a significant impact on the flutter predictions of various transonic wing and aircraft configurations.[2,3] When nonlinearities are present, the amplitude of oscillations can become limited and limit cycle oscillations (LCO) are observed. This is a problem of considerable practical interest and is well documented for *in-service* aircraft.[4,5]

The presence of nonlinearities, either structural or aerodynamic, poses additional challenges both in terms of complexity and computational resources, these requirements can be exacerbated by the need for probabilistic analysis. Hence, to address this issue, a Harmonic Balance (HB) based method is implemented for the LCO simulation. The HB method can offer over one order of magnitude reduction in computational effort when compared against time domain methods.[5–8] An overview of different variations of the Harmonic Balance method, such as high-dimensional, incremental, or elliptic HB methods is given by Dimitriadis.[9]

Here the HB CFD solver is based on the Euler equations and follows the high-dimensional HB formulation developed by Hall *et al*.[10] The CFD-CSD coupling is performed through the communication of aerodynamic forces and structural displacements between the CFD solver and structural equations. The probabilistic analysis is based on non-intrusive polynomial chaos expansions (PCE) which offer an attractive technique for uncertainty quantification at a reduced cost with respect to Monte Carlo analysis.[11] PCE has been successfully applied to aeroelastic problems including the uncertainty quantification of LCO predictions.[12,13]

In this work, a description of the CFD flow solver and aeroelastic equations of motion is presented. Following this the implementation of the Harmonic Balance method is described. The HB formulation is applied in conjunction with the PCE to investigate the stochastic response of a 2 *dof* aerofoil when subject to uncertainties in aerodynamic and structural parameters. Results consist of:- firstly, aerodynamic parameters are investigated such as velocity and altitude, secondly, structural variability is included in a variety of forms.

II. Harmonic Balance CFD Flow Solver

II.A. Flow equations

The flow solver used in this work follows that described by Yao and Marques.[14] Consider the semi-discrete form of the three-dimensional Euler equations:

$$\frac{\partial \mathbf{W}}{\partial t} = -\mathbf{R}(\mathbf{W}) \tag{1}$$

where $\mathbf{R}$ is the residual error of the steady-state solution:

$$\mathbf{R} = \frac{\partial \mathbf{F}}{\partial x} + \frac{\partial \mathbf{G}}{\partial y} + \frac{\partial \mathbf{H}}{\partial z} \tag{2}$$

$\mathbf{W}$ represents the vector of conserved variables and $\mathbf{F}$, $\mathbf{G}$ and $\mathbf{H}$ are the fluxes in each direction, ie.

$$\mathbf{W} = \begin{Bmatrix} \rho \\ \rho u \\ \rho v \\ \rho w \\ \rho E \end{Bmatrix}, \quad \mathbf{F} = \begin{Bmatrix} \rho u \\ \rho uu + p \\ \rho uv \\ \rho uw \\ u(\rho E + p) \end{Bmatrix}, \quad \mathbf{G} = \begin{Bmatrix} \rho v \\ \rho uv \\ \rho vv + p \\ \rho vw \\ v(\rho E + p) \end{Bmatrix}, \quad \mathbf{H} = \begin{Bmatrix} \rho w \\ \rho uw \\ \rho vw \\ \rho ww + p \\ w(\rho E + p) \end{Bmatrix}$$

Equation (1) is solved by marching forward in time implicitly by solving the discrete nonlinear set of equations:

$$\frac{\mathbf{W}^{n+1} - \mathbf{W}^n}{\Delta t} = -\mathbf{R}\left(\mathbf{W}^{n+1}\right) \tag{3}$$

with the residual at the next time step, $\mathbf{R}^{n+1}$ approximated by linearisation with respect to time, t:

$$\mathbf{R}^{n+1} \approx \mathbf{R}^n + \frac{\partial \mathbf{R}}{\partial \mathbf{W}} \Delta \mathbf{W} \tag{4}$$

where $\Delta\mathbf{W} = \mathbf{W}^{n+1} - \mathbf{W}^n$. The convective flux terms contained in the residual, $\mathbf{R}$ are discretised using a Roe flux function[15] and *MUSCL* extrapolation[16] to achieve 2^{nd} order accuracy with a Van Albada limiter in place to ensure monotonic solutions around shock waves.[17] The solution of eq. (3) is found using a *LUSGS* scheme.[18]

II.B. Harmonic Balance Formulation

The implementation of the HB is described by Woodgate and Badcock[19] and is summarised next. Consider the semi-discrete form of eq. (1) as a system of ordinary differential equations:

$$\mathbf{I}(t) = \frac{d\mathbf{W}(t)}{dt} + \mathbf{R}(t) = 0 \tag{5}$$

Assuming periodicity, the solution, $\mathbf{W}$ and residual, $\mathbf{R}$ of eq. (5) can be represented as truncated Fourier series with N_H harmonics and a fundamental frequency ω.

$$\mathbf{W}(t) \approx \hat{\mathbf{W}}_0 + \sum_{n=1}^{N_H} (\hat{\mathbf{W}}_{2n-1}\cos(n\omega t) + \hat{\mathbf{W}}_{2n}\sin(n\omega t)) \tag{6}$$

$$\mathbf{R}(t) \approx \hat{\mathbf{R}}_0 + \sum_{n=1}^{N_H} (\hat{\mathbf{R}}_{2n-1}\cos(n\omega t) + \hat{\mathbf{R}}_{2n}\sin(n\omega t)) \tag{7}$$

Likewise, eq. (5) can also be expressed as a Fourier series as:

$$\mathbf{I}(t) \approx \hat{\mathbf{I}}_0 + \sum_{n=1}^{N_H} (\hat{\mathbf{I}}_{2n-1}\cos(n\omega t) + \hat{\mathbf{I}}_{2n}\sin(n\omega t)) \tag{8}$$

The orthogonality of the Fourier series allows the *balancing* of individual harmonics leading to:

$$\hat{\mathbf{I}}_0 = \hat{\mathbf{R}}_0 = 0 \tag{9}$$

$$\hat{\mathbf{I}}_{2n-1} = \omega n\hat{\mathbf{W}}_{2n} + \hat{\mathbf{R}}_{2n-1} = 0 \tag{10}$$

$$\hat{\mathbf{I}}_{2n} = -\omega n\hat{\mathbf{W}}_{2n+1} + \hat{\mathbf{R}}_{2n} = 0 \tag{11}$$

This is a system of $2N_H + 1$ equations and can conveniently be expressed in matrix form:

$$\omega\mathbf{A}\hat{\mathbf{W}} + \hat{\mathbf{R}} = \mathbf{0} \tag{12}$$

where $\hat{\mathbf{W}}$ and $\hat{\mathbf{R}}$ are the vectors of Fourier coefficients. $\mathbf{A}$ can be found in reference.[7] To avoid to expressing the Fourier coefficients in $\hat{\mathbf{R}}$ as functions of $\hat{\mathbf{W}}$ the system is cast back into the time domain as proposed by Hall *et al.*[10] The Fourier coefficients are related to time domain solutions using a constant transformation matrix which yields:

$$\hat{\mathbf{W}} = \mathbf{E}\mathbf{W}_{hb} \quad \hat{\mathbf{R}} = \mathbf{E}\mathbf{R}_{hb} \tag{13}$$

where $\mathbf{W}_{hb}$ and $\mathbf{R}_{hb}$ represent the flow variable and residual values at $2N_H + 1$ discrete, equally spaced time intervals over one temporal period. The transformation matrix, $\mathbf{E}$ is also found in reference.[7] Substituting the terms in eq. (13) into (12) and pre-multiplying by $\mathbf{E}^{-1}$ yields:

$$\omega\mathbf{D}\mathbf{W}_{hb} + \mathbf{R}_{hb} = \mathbf{0} \tag{14}$$

where $\mathbf{D} = \mathbf{E}^{-1}\mathbf{A}\mathbf{E}$, the elements in $\mathbf{D}$ can be defined as:

$$\mathbf{D}_{i,j} = \frac{2}{2N_H + 1}\sum_{k=1}^{N_H}\left[k\,\sin\left(\frac{2\pi k(j-i)}{2N_H+1}\right)\right] \tag{15}$$

A pseudo time derivative term is added to allow eq. (14) to be pseudo time-marched to convergence:

$$\frac{d\mathbf{W}_{hb}}{d\tau} + \omega\mathbf{D}\mathbf{W}_{hb} + \mathbf{R}_{hb} = 0 \tag{16}$$

As mentioned earlier a *LUSGS* scheme is employed in this work. Note that the Fourier coefficients still can be obtained by pre-multiplying solution vector by the transformation matrix, $\mathbf{E}$ and the flow field at any discrete time point throughout the oscillation period can be found by reconstructing the Fourier series and evaluating it for the desired time value.

III. Aeroelastic Formulation

The equations of motion for a pitch/plunge aerofoil system with no damping as described by Yao and Marques[14] can be expressed as:

$$\mathbf{M}\ddot{\mathbf{y}} + \frac{1}{V^2}\mathbf{K}\mathbf{y} = \mathbf{E}_f\mathbf{f} \tag{17}$$

where:

$$\mathbf{M} = \begin{bmatrix} 1 & x_\alpha \\ x_\alpha & r_\alpha^2 \end{bmatrix}, \quad \mathbf{K} = \begin{bmatrix} (\omega_h/\omega_\alpha)^2 & 0 \\ 0 & r_\alpha^2 \end{bmatrix}, \quad \mathbf{E}_f = \begin{bmatrix} -4/\pi\mu & 0 \\ 0 & 8/\pi\mu \end{bmatrix}, \quad \mathbf{f} = \begin{Bmatrix} C_l \\ C_m \end{Bmatrix}, \quad \mathbf{y} = \begin{Bmatrix} h/b \\ \alpha \end{Bmatrix}$$

Equation (17) can be transformed into state-space form:

$$\dot{\mathbf{Y}} = \mathbf{A_s}\mathbf{Y} + \mathbf{B_s}\mathbf{F} \tag{18}$$

where:

$$\mathbf{Y} = \begin{Bmatrix} \mathbf{y} \\ \dot{\mathbf{y}} \end{Bmatrix}, \quad \mathbf{A_s} = \begin{bmatrix} \mathbf{0} & \mathbf{I} \\ \frac{-1}{V^2}\mathbf{M}^{-1}\mathbf{K} & \mathbf{0} \end{bmatrix}, \quad \mathbf{B_s} = \begin{bmatrix} \mathbf{0} & \mathbf{0} \\ \mathbf{0} & \mathbf{M}^{-1}\mathbf{E}_f \end{bmatrix}, \quad \mathbf{F} = \begin{Bmatrix} \mathbf{0} \\ \mathbf{f} \end{Bmatrix}$$

Applying the Harmonic Balance formulation to Eq. (18) gives:

$$\omega\mathbf{D}\mathbf{Y}_{hb} - (\mathbf{A_s}\mathbf{Y}_{hb} + \mathbf{B_s}\mathbf{F}) = 0 \tag{19}$$

where $\mathbf{D}$ is the same HB operator as described before. Again, as in eq. (16) pseudo time marching is used to solve eq. (19):

$$\frac{d\mathbf{Y}_{hb}}{d\tau} + \omega\mathbf{D}\mathbf{Y}_{hb} - (\mathbf{A_s}\mathbf{Y}_{hb} + \mathbf{B_s}\mathbf{F}) = 0 \tag{20}$$

Equation (16) together with eq. (20) represent the nonlinear coupled aeroelastic system. When solving the aeroelastic system of equations, at each iteration, the generalised aerodynamic forces are computed using eq. (16), which will feed into eq. (20). The solution from eq. (20) will provide new generalised displacement and grid velocities to eq. (16). To find the LCO condition, eq. (20) is solved for a given combination of $[\omega, \mathbf{f}]$, then transfer the displacements back to the fluid system. The frequency is updated by minimising the $L2$ norm of the residual of eq. (20), using the following expression:

$$\frac{\partial\mathbf{L}_n}{\partial\omega} = \left(\omega\mathbf{D}\mathbf{Y}_{hb} - \frac{\partial\mathbf{F}}{\partial\omega}\right)^{\mathrm{T}} [\omega\mathbf{D}\mathbf{Y}_{hb} - (\mathbf{A_s}\mathbf{Y}_{hb} + \mathbf{B_s}\mathbf{F})] \tag{21}$$

where $\partial\mathbf{L}_n/\partial\omega$ is the derivative of the $L2$ norm with respect to the frequency, ω. The frequency is updated every n_i iterations. This reduces the amount of expensive computations of the derivative term, $\partial\mathbf{F}/\partial\omega$ thus reducing the computational cost.

IV. Results

IV.A. HB Validation

For validation of the HB solver, comparisons were made against the time domain solutions presented by Yao and Marques.[14] Figure 1 shows the performance of the aeroelastic HB solver with different numbers of harmonics. Three harmonics are needed to accuracy replicate the time domain result, however one harmonic gives a reasonable approximation of the response and is employed throughout the remainder of this work. The behaviour in Fig. 1 represents supercritical LCO growth and is observed with increasing *Velocity Index* which is given by:

$$V_s = \frac{U_\infty}{b\omega_\alpha\sqrt{\mu}} \tag{22}$$

The definition of the *Velocity Index* relates both aerodynamic and structural properties of the problem and the response of the system when changed depends on what components within eq. (22) remain constant. In this case the supercritical LCO is generated by a change in natural frequency in the pitch *dof*, ω_α. For the remainder of this work, we consider the highest amplitude point in Fig. 1 as the deterministic case which uncertainty is imposed ie. ω_α remains constant. The input parameters for this deterministic condition are shown in Table 1.

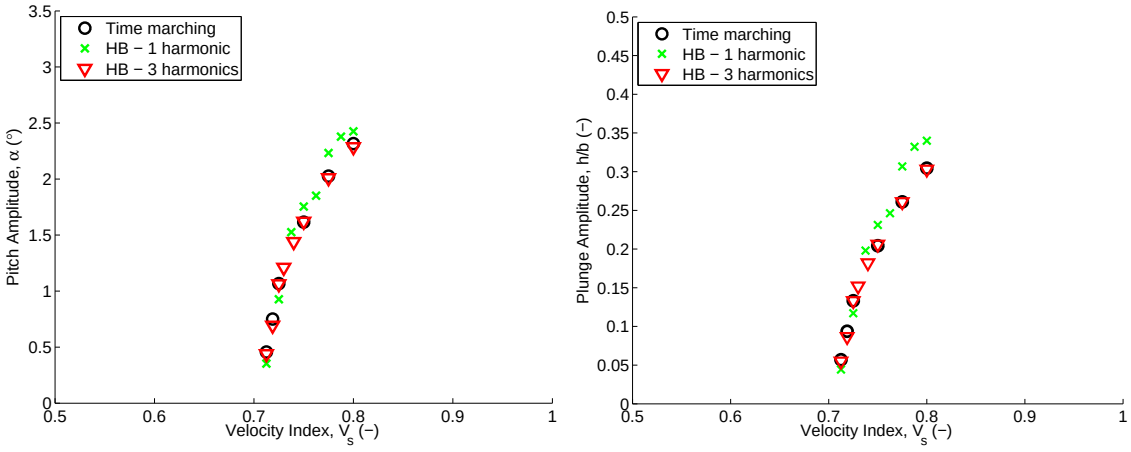

(a) LCO pitch amplitude vs. Velocity index

(b) LCO plunge amplitude vs. Velocity index

Figure 1. Comparison of HB and time marching solutions at *Mach no. = 0.8*

Table 1. Deterministic parameters

Parameter	Value
Static unbalance, x_α	0.25
Radius of gyration about elastic axis, ${r_\alpha}^2$	0.75
Distance from elastic axis to centre chord, a_h/b	-0.6
Frequency ratio, ω_h/ω_α	0.5
Mach number, M	0.8
Speed of sound	340.294
Mass ratio, μ	75
Velocity index, V_s	0.8

IV.B. Aerodynamic Variability

Uncertainty in the airflow can have a significant impact on the movement of the aerofoil. Here we consider two aerodynamic parameters:- the density and the Mach number/velocity. Uniform distributions are applied to all uncertain parameters and 5th order polynomial chaos expansions using 82 samples are used. Figures 2(a) and 2(b) shows the effects of a $\pm 10\%$ variation in free-stream density and Figs 2(c) and 2(d) show a $\pm 1\%$ variation in Mach number/velocity. Results for plunge are not shown in this work as they follow the same trends as the results for pitch.

The changes in density scale the aerodynamic forces acting on the aerofoil but do not affect the flow-features. As a result, an almost linear relationship between amplitude and density is exhibited, a $\pm 10\%$ change in density induces a similar change in LCO amplitude, $^{+9.70\%}_{-8.23\%}$ on the deterministic amplitude of 2.427°. When Mach number is varied, a much greater change in amplitude is observed. A $\pm 1\%$ variation produces a $^{+35.8\%}_{-61.2\%}$ effect on amplitude emphasising how sensitive the aeroelastic interaction is to Mach number. The decrease in amplitude caused by an increase in Mach number is counter-intuitive; as the Mach number increases, the shock wave shifts backwards and changes the position of centre of force with respect to the elastic axis of the aerofoil, this changes the pitching moment and increases the stability of the aerofoil in a quadratic manner. The growth and translation of the shock wave is visible in Fig. 3.

As the density does not change the aerodynamic forces in a nonlinear manner only the Mach number will be considered when the structural variability is introduced.

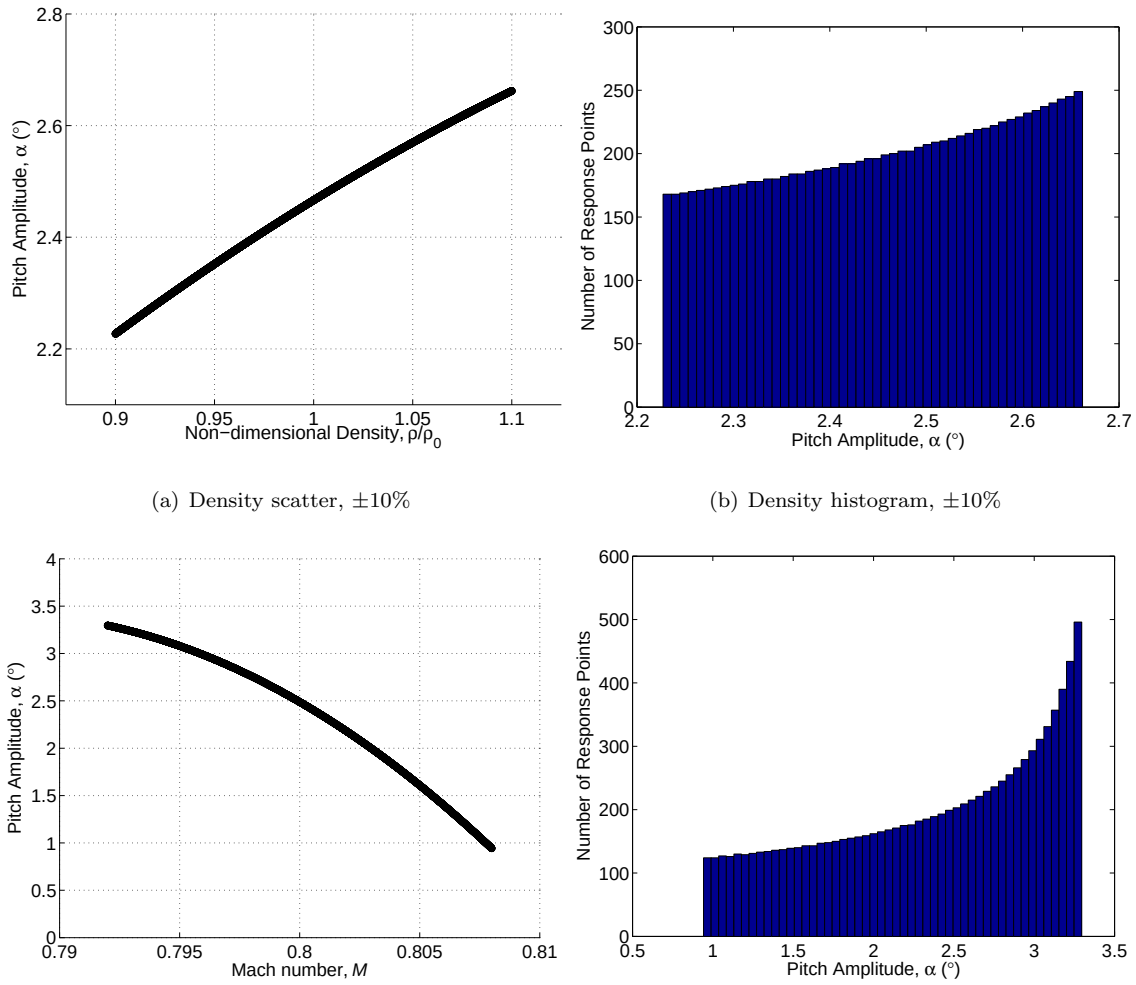

(a) Density scatter, ±10%

(b) Density histogram, ±10%

(c) Mach no. scatter, ±1%

(d) Mach no. histogram, ±1%

Figure 2. Aerofoil behaviour subject to aerodynamic uncertainty. PCE, $\mathcal{O} = 5, 82$ samples

IV.C. Structural Variability

Structural uncertainty is applied to three different parameters in this section:- radius of gyration, ${r_\alpha}^2$, static unbalance, x_α and frequency ratio, ω_h/ω_α. All cases include the ±1% variability imposed on Mach no and the deterministic values are shown in Table 1.

The radius of gyration, ${r_\alpha}^2$ quantifies distance between the elastic axis and the centre of gravity. Variability of ±33% was assigned to ${r_\alpha}^2$ and a supercritical bifurcation is observed as a result. The presence of the bifurcation point can adversely affect the performance of the PCE so to mitigate this, adaptive sampling is employed.[13] The response surface of the LCO pitch amplitude is shown in Fig. 4 and it is clear the bifurcation boundary is well defined.

The static unbalance, x_α is subject to ±20% uncertainty and also exhibits a supercritical bifurcation as shown in Fig. 5. The response of the aerofoil resembles that shown in Fig. 4 with a similarly defined bifurcation boundary which takes a quadratic form. This is caused by the nonlinear effects of the Mach number variability.

The final structural parameter to be investigated is the frequency ratio, ω_h/ω_α and is shown in Fig. 6. Variability of ±20% is imposed. As the natural frequency in pitch is constant, effectively only the frequency in plunge is changing. The bifurcation boundary line in this case is of a different form than previously shown. The frequency ratio interacts with the Mach number creating an 'S' shape boundary line, however the PCE is still able to produce the well-defined bifurcation. The interaction between these two parameters is not fully understood and needs further attention.

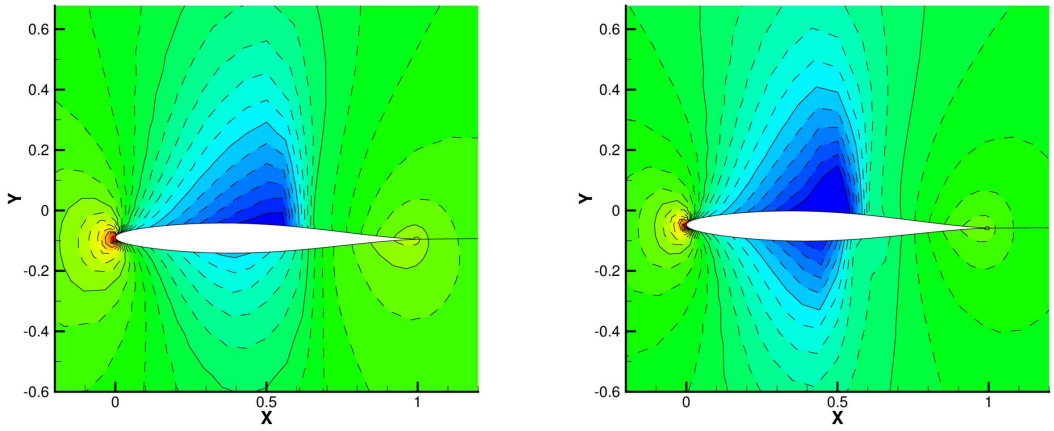

(a) Mach no., $M = 0.792$, pitch, $\alpha = 0.65°$ (b) Mach no., $M = 0.808$, pitch, $\alpha = 0.65°$

Figure 3.

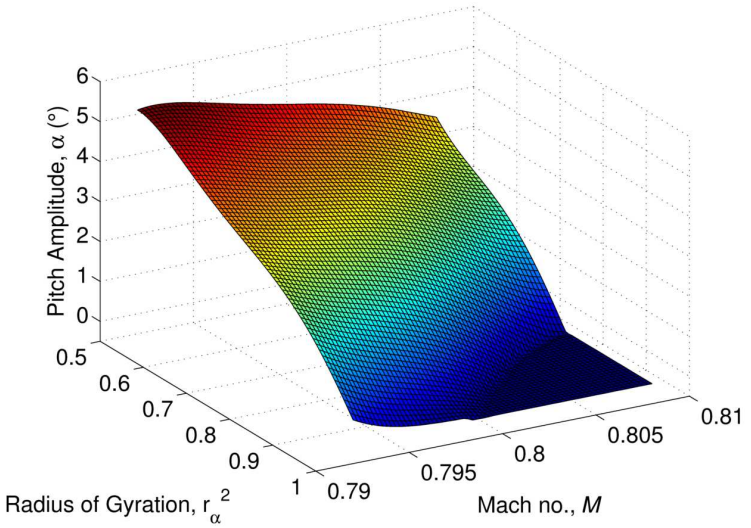

Figure 4. Supercritical bifurcation with varying Mach no. and $r_\alpha{}^2$

V. Conclusions & Outlook

The impact of variability in both structural and aerodynamic parameters on a two degree of freedom aerofoil is investigated. An Euler-based CFD code is coupled with a linear aeroelastic model and a Harmonic Balance method is implemented. Polynomial Chaos Expansions are employed for the stochastic analysis with adaptive sampling utilised in the presence of discontinuities at the bifurcation boundaries. The LCO amplitude in the pitch degree of freedom is shown when variability is applied to density and Mach number demonstrating the sensitivity associated with Mach number. The structural variability is then combined with the uncertainty in Mach number in the form of:- radius of gyration, static unbalance and frequency ratio. All cases exhibit supercritical bifurcations and show different shapes of bifurcation boundaries. These cases need looked at in more detail to understand the interactions between the structural and aerodynamic parameters and how this shapes the bifurcation boundary. Other further work consists of the inclusion of structural nonlinearities to allow the analysis of subcritical bifurcations.

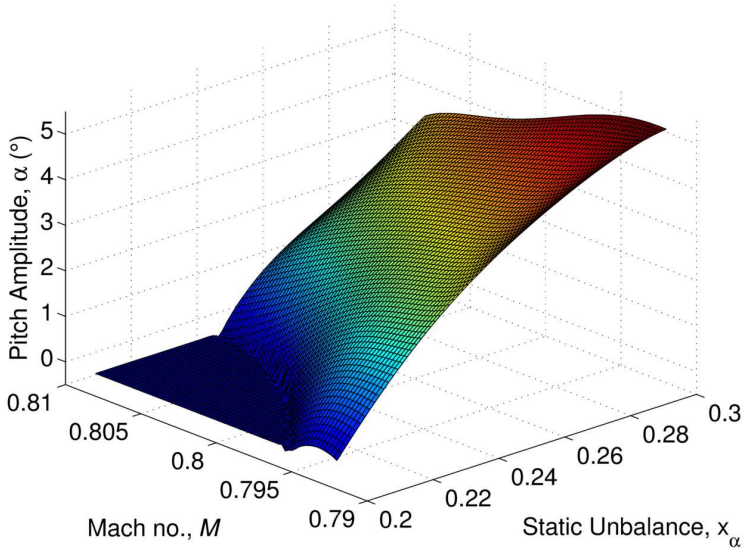

Figure 5. Supercritical bifurcation with varying Mach no. and $x_\alpha{}^2$

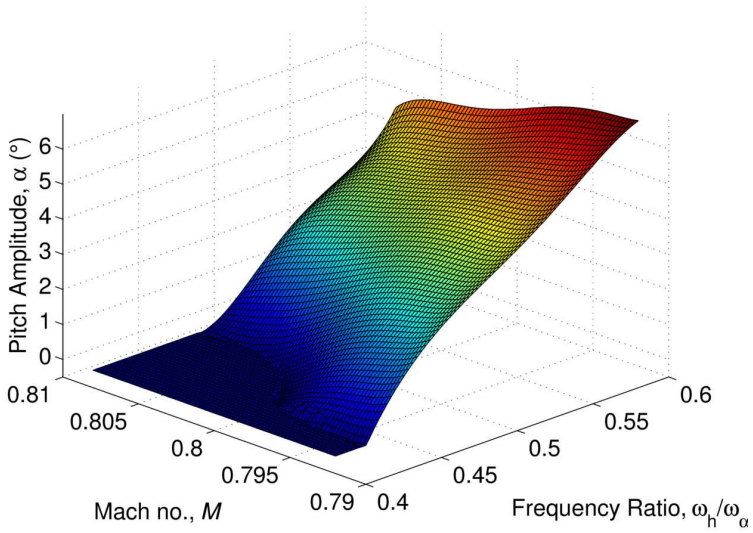

Figure 6. Supercritical bifurcation with varying Mach no. and frequency ratio

Acknowledgments

The funding provided for this research from the Department of Education and Learning (DEL) is gratefully acknowledged.

References

[1]C. Pettit, Uncertainty Quantification in Aeroelasticity: Recent Results and Research Challenges, Journal of Aircraft 41 (5) (2004) 1217–1229.

[2]S. Marques, K. Badcock, H. Khodaparast, J. Mottershead, Transonic Aeroelastic Stability Predictions Under the Influence of Structural Variability, Journal of Aircraft 47 (4) (2010) 1229–1239.

[3]S. Marques, K. Badcock, H. Khodaparast, J. Mottershead, How Structural Model Variability Influences Transonic Aeroelastic Stability, Journal of Aircraft 49 (5) (2012) 1189–1199. doi:10.2514/1.C031103.

[4]R. Bunton, C. Denegri, Limit Cycle Oscillation Characteristics of Fighter Aircraft, Journal of Aircraft 37 (5) (2000) 916–918.

[5]J. Thomas, E. Dowell, K. Hall, C. Denegri, Modeling Limit Cycle Oscillation Behavior of the F-16 Fighter Using a

Harmonic Balance Approach (AIAA-2004-1696), presented at the 45th AIAA/ASME/ASCE/AHS/ASC Structures, Structural Dynamics, and Materials Conference, Palm Springs, California.

[6]A. Gopinath, P. Beran, A. Jameson, Comparative Analysis of Computational Methods for Limit-Cycle Oscillations (AIAA-2006-2076), presented at the 47th AIAA/ASME/ASCE/AHS/ASC Structures, Structural Dynamics and Materials Conference, Newport, Rhode Island.

[7]L. Liu, E. Dowell, J. Thomas, A high dimensional harmonic balance approach for an aeroelastic airfoil with cubic restoring forces, Journal of Fluids and Structures 23 (3) (2007) 351–363. doi:10.1016/j.jfluidstructs.2006.09.005.

[8]G. Dimitriadis, G. Vio, J. Cooper, Application of Higher-Order Harmonic Balance to Non-Linear Aeroelastic Systems (AIAA-2006-2023), presented at the 47th AIAA/ASME/ASCE/AHS/ASC Structures, Structural Dynamics, and Materials Conference, Newport, Rhode Island.

[9]G. Dimitriadis, Continuation of Higher-Order Harmonic Balance Solutions for Nonlinear Aeroelastic Systems, Journal of Aircraft 45 (2) (2008) 523–537. doi:10.2514/1.30472.

[10]K. Hall, J. Thomas, W. Clark, Computation of Unsteady Nonlinear Flows in Cascades Using a Harmonic Balance Technique, AIAA Journal 40 (5) (2002) 879–886.

[11]M. Eldred, Recent Advances in Non-Intusive Polynomial Chaos and Stochastic Collocation Methods for Uncertainty Analysis and Design (AIAA-2009-2274), presented at the 50th AIAA/ASME/ASCE/AHS/ASC Structures, Structural Dynamics, and Materials Conference, Palm Springs, California.

[12]P. Beran, C. Pettit, A Direct Method for Quantifying Limit-Cycle Oscillation Response Characteristics in the Presence of Uncertainties.

[13]J. L. Meitour, D. Lucor, C. Chassaing, Prediction of stochastic limit cycle oscillations using an adaptive Polynomial Chaos method, Journal of Aeroelasticity and Structural Dynamics 2 (1) (2010) 3–22.

[14]W. Yao, S. Marques, Prediction of Transonic Limit Cycle Oscillations using an Aeroelastic Harmonic Balance Method, AIAA journal 53, accepted for publication September 2014.

[15]P. Roe, Approximate Riemann Solvers, Parameter Vectors, and Difference Schemes, Journal of Computational Physics 43 (1981) 357–372.

[16]B. V. Leer, The Ultimate Conservative Difference Scheme II: Monotonicity and Conservative Combined in a Second Order Scheme, Journal of Computational Physics 14 (4) (1974) 361–374.

[17]L. Dubuc, F. Cantariti, M. Woodgate, B. Gribben, K. Badcock, B. Richards, Solution of the Unsteady Euler Equations Using an Implicit Dual-Time Method, AIAA Journal 36 (8) (1998) 1417–1424.

[18]S. Yoon, A. Jameson, Lower-Upper Symmetric-Gauss-Seidel Method for the Euler and Navier-Stokes Equations, AIAA Journal 26 (9).

[19]M. Woodgate, K. Badcock, Implicit Harmonic Balance Solver for Transonic Flow with Forced Motions, AIAA Journal 47 (4).